First observations of $h_c \to$ hadrons

M. Ablikim,[1] M. N. Achasov,[10,d] P. Adlarson,[59] S. Ahmed,[15] M. Albrecht,[4] M. Alekseev,[58a,58c] A. Amoroso,[58a,58c] F. F. An,[1] Q. An,[55,43] Y. Bai,[42] O. Bakina,[27] R. Baldini Ferroli,[23a] I. Balossino,[24a] Y. Ban,[35] K. Begzsuren,[25] J. V. Bennett,[5] N. Berger,[26] M. Bertani,[23a] D. Bettoni,[24a] F. Bianchi,[58a,58c] J. Biernat,[59] J. Bloms,[52] I. Boyko,[27] R. A. Briere,[5] H. Cai,[60] X. Cai,[1,43] A. Calcaterra,[23a] G. F. Cao,[1,47] N. Cao,[1,47] S. A. Cetin,[46b] J. Chai,[58c] J. F. Chang,[1,43] W. L. Chang,[1,47] G. Chelkov,[27,b,c] D. Y. Chen,[6] G. Chen,[1] H. S. Chen,[1,47] J. C. Chen,[1] M. L. Chen,[1,43] S. J. Chen,[33] Y. B. Chen,[1,43] W. Cheng,[58c] G. Cibinetto,[24a] F. Cossio,[58c] X. F. Cui,[34] H. L. Dai,[1,43] J. P. Dai,[38,h] X. C. Dai,[1,47] A. Dbeyssi,[15] D. Dedovich,[27] Z. Y. Deng,[1] A. Denig,[26] I. Denysenko,[27] M. Destefanis,[58a,58c] F. De Mori,[58a,58c] Y. Ding,[31] C. Dong,[34] J. Dong,[1,43] L. Y. Dong,[1,47] M. Y. Dong,[1,43,47] Z. L. Dou,[33] S. X. Du,[63] J. Z. Fan,[45] J. Fang,[1,43] S. S. Fang,[1,47] Y. Fang,[1] R. Farinelli,[24a,24b] L. Fava,[58b,58c] F. Feldbauer,[4] G. Felici,[23a] C. Q. Feng,[55,43] M. Fritsch,[4] C. D. Fu,[1] Y. Fu,[1] Q. Gao,[1] X. L. Gao,[55,43] Y. Gao,[45] Y. Gao,[56] Y. G. Gao,[6] Z. Gao,[55,43] B. Garillon,[26] I. Garzia,[24a] E. M. Gersabeck,[50] A. Gilman,[51] K. Goetzen,[11] L. Gong,[34] W. X. Gong,[1,43] W. Gradl,[26] M. Greco,[58a,58c] L. M. Gu,[33] M. H. Gu,[1,43] S. Gu,[2] Y. T. Gu,[13] A. Q. Guo,[22] L. B. Guo,[32] R. P. Guo,[36] Y. P. Guo,[26] A. Guskov,[27] S. Han,[60] X. Q. Hao,[16] F. A. Harris,[48] K. L. He,[1,47] F. H. Heinsius,[4] T. Held,[4] Y. K. Heng,[1,43,47] M. Himmelreich,[11,g] Y. R. Hou,[47] Z. L. Hou,[1] H. M. Hu,[1,47] J. F. Hu,[38,h] T. Hu,[1,43,47] Y. Hu,[1] G. S. Huang,[55,43] J. S. Huang,[16] X. T. Huang,[37] X. Z. Huang,[33] N. Huesken,[52] T. Hussain,[57] W. Ikegami Andersson,[59] W. Imoehl,[22] M. Irshad,[55,43] Q. Ji,[1] Q. P. Ji,[16] X. B. Ji,[1,47] X. L. Ji,[1,43] H. L. Jiang,[37] X. S. Jiang,[1,43,47] X. Y. Jiang,[34] J. B. Jiao,[37] Z. Jiao,[18] D. P. Jin,[1,43,47] S. Jin,[33] Y. Jin,[49] T. Johansson,[59] N. Kalantar-Nayestanaki,[29] X. S. Kang,[31] R. Kappert,[29] M. Kavatsyuk,[29] B. C. Ke,[1] I. K. Keshk,[4] A. Khoukaz,[52] P. Kiese,[26] R. Kiuchi,[1] R. Kliemt,[11] L. Koch,[28] O. B. Kolcu,[46b,f] B. Kopf,[4] M. Kuemmel,[4] M. Kuessner,[4] A. Kupsc,[59] M. Kurth,[1] M. G. Kurth,[1,47] W. Kühn,[28] J. S. Lange,[28] P. Larin,[15] L. Lavezzi,[58c] H. Leithoff,[26] T. Lenz,[26] C. Li,[59] Cheng Li,[55,43] D. M. Li,[63] F. Li,[1,43] F. Y. Li,[35] G. Li,[1] H. B. Li,[1,47] H. J. Li,[9,j] J. C. Li,[1] J. W. Li,[41] Ke Li,[1] L. K. Li,[1] Lei Li,[3] P. L. Li,[55,43] P. R. Li,[30] Q. Y. Li,[37] W. D. Li,[1,47] W. G. Li,[1] X. H. Li,[55,43] X. L. Li,[37] X. N. Li,[1,43] Z. B. Li,[44] Z. Y. Li,[44] H. Liang,[55,43] H. Liang,[1,47] Y. F. Liang,[40] Y. T. Liang,[28] G. R. Liao,[12] L. Z. Liao,[1,47] J. Libby,[21] C. X. Lin,[44] D. X. Lin,[15] Y. J. Lin,[13] B. Liu,[38,h] B. J. Liu,[1] C. X. Liu,[1] D. Liu,[55,43] D. Y. Liu,[38,h] F. H. Liu,[39] Fang Liu,[1] Feng Liu,[6] H. B. Liu,[13] H. M. Liu,[1,47] Huanhuan Liu,[1] Huihui Liu,[17] J. B. Liu,[55,43] J. Y. Liu,[1,47] K. Y. Liu,[31] Ke Liu,[6] L. Y. Liu,[13] Q. Liu,[47] S. B. Liu,[55,43] T. Liu,[1,47] X. Liu,[30] X. Y. Liu,[1,47] Y. B. Liu,[34] Z. A. Liu,[1,43,47] Zhiqing Liu,[37] Y. F. Long,[35] X. C. Lou,[1,43,47] H. J. Lu,[18] J. D. Lu,[1,47] J. G. Lu,[1,43] Y. Lu,[1] Y. P. Lu,[1,43] C. L. Luo,[32] M. X. Luo,[62] P. W. Luo,[44] T. Luo,[9,j] X. L. Luo,[1,43] S. Lusso,[58c] X. R. Lyu,[47] F. C. Ma,[31] H. L. Ma,[1] L. L. Ma,[37] M. M. Ma,[1,47] Q. M. Ma,[1] X. N. Ma,[34] X. X. Ma,[1,47] X. Y. Ma,[1,43] Y. M. Ma,[37] F. E. Maas,[15] M. Maggiora,[58a,58c] S. Maldaner,[26] S. Malde,[53] Q. A. Malik,[57] A. Mangoni,[23b] Y. J. Mao,[35] Z. P. Mao,[1] S. Marcello,[58a,58c] Z. X. Meng,[49] J. G. Messchendorp,[29] G. Mezzadri,[24a] J. Min,[1,43] T. J. Min,[33] R. E. Mitchell,[22] X. H. Mo,[1,43,47] Y. J. Mo,[6] C. Morales Morales,[15] N. Yu. Muchnoi,[10,d] H. Muramatsu,[51] A. Mustafa,[4] S. Nakhoul,[11,g] Y. Nefedov,[27] F. Nerling,[11,g] I. B. Nikolaev,[10,d] Z. Ning,[1,43] S. Nisar,[8,k] S. L. Niu,[1,43] S. L. Olsen,[47] Q. Ouyang,[1,43,47] S. Pacetti,[23b] Y. Pan,[55,43] M. Papenbrock,[59] P. Patteri,[23a] M. Pelizaeus,[4] H. P. Peng,[55,43] K. Peters,[11,g] J. Pettersson,[59] J. L. Ping,[32] R. G. Ping,[1,47] A. Pitka,[4] R. Poling,[51] V. Prasad,[55,43] H. R. Qi,[2] M. Qi,[33] T. Y. Qi,[2] S. Qian,[1,43] C. F. Qiao,[47] N. Qin,[60] X. P. Qin,[13] X. S. Qin,[4] Z. H. Qin,[1,43] J. F. Qiu,[1] S. Q. Qu,[34] K. H. Rashid,[57,i] K. Ravindran,[21] C. F. Redmer,[26] M. Richter,[4] A. Rivetti,[58c] V. Rodin,[29] M. Rolo,[58c] G. Rong,[1,47] Ch. Rosner,[15] M. Rump,[52] A. Sarantsev,[27,e] M. Savrié,[24b] Y. Schelhaas,[26] K. Schoenning,[59] W. Shan,[19] X. Y. Shan,[55,43] M. Shao,[55,43] C. P. Shen,[2] P. X. Shen,[34] X. Y. Shen,[1,47] H. Y. Sheng,[1] X. Shi,[1,43] X. D. Shi,[55,43] J. J. Song,[37] Q. Q. Song,[55,43] X. Y. Song,[1] S. Sosio,[58a,58c] C. Sowa,[4] S. Spataro,[58a,58c] F. F. Sui,[37] G. X. Sun,[1] J. F. Sun,[16] L. Sun,[60] S. S. Sun,[1,47] X. H. Sun,[1] Y. J. Sun,[55,43] Y. K. Sun,[55,43] Y. Z. Sun,[1] Z. J. Sun,[1,43] Z. T. Sun,[1] Y. T. Tan,[55,43] C. J. Tang,[40] G. Y. Tang,[1] X. Tang,[1] V. Thoren,[59] B. Tsednee,[25] I. Uman,[46d] B. Wang,[1] B. L. Wang,[47] C. W. Wang,[33] D. Y. Wang,[35] K. Wang,[1,43] L. L. Wang,[1] L. S. Wang,[1] M. Wang,[37] M. Z. Wang,[35] Meng Wang,[1,47] P. L. Wang,[1] R. M. Wang,[61] W. P. Wang,[55,43] X. Wang,[35] X. F. Wang,[1] X. L. Wang,[9,j] Y. Wang,[55,43] Y. Wang,[44] Y. F. Wang,[1,43,47] Z. Wang,[1,43] Z. G. Wang,[1,43] Z. Y. Wang,[1] Zongyuan Wang,[1,47] T. Weber,[4] D. H. Wei,[12] P. Weidenkaff,[26] H. W. Wen,[32] S. P. Wen,[1] U. Wiedner,[4] G. Wilkinson,[53] M. Wolke,[59] L. H. Wu,[1] L. J. Wu,[1,47] Z. Wu,[1,43] L. Xia,[55,43] Y. Xia,[20] S. Y. Xiao,[1] Y. J. Xiao,[1,47] Z. J. Xiao,[32] Y. G. Xie,[1,43] Y. H. Xie,[6] T. Y. Xing,[1,47] X. A. Xiong,[1,47] Q. L. Xiu,[1,43] G. F. Xu,[1] J. J. Xu,[33] L. Xu,[1] Q. J. Xu,[14] W. Xu,[1,47] X. P. Xu,[41] F. Yan,[56] L. Yan,[58a,58c] W. B. Yan,[55,43] W. C. Yan,[2] Y. H. Yan,[20] H. J. Yang,[38,h] H. X. Yang,[1] L. Yang,[60] R. X. Yang,[55,43] S. L. Yang,[1,47] Y. H. Yang,[33] Y. X. Yang,[12] Yifan Yang,[1,47] Z. Q. Yang,[20] M. Ye,[1,43] M. H. Ye,[7] J. H. Yin,[1] Z. Y. You,[44] B. X. Yu,[1,43,47] C. X. Yu,[34] J. S. Yu,[20] T. Yu,[56] C. Z. Yuan,[1,47] X. Q. Yuan,[35] Y. Yuan,[1] A. Yuncu,[46b,a] A. A. Zafar,[57] Y. Zeng,[20] B. X. Zhang,[1] B. Y. Zhang,[1,43] C. C. Zhang,[1] D. H. Zhang,[1] H. H. Zhang,[44] H. Y. Zhang,[1,43] J. Zhang,[1,47] J. L. Zhang,[61] J. Q. Zhang,[4] J. W. Zhang,[1,43,47] J. Y. Zhang,[1] J. Z. Zhang,[1,47] K. Zhang,[1,47] L. Zhang,[45] S. F. Zhang,[33]

072008-1

T. J. Zhang,[38,h] X. Y. Zhang,[37] Y. Zhang,[55,43] Y. H. Zhang,[1,43] Y. T. Zhang,[55,43] Yang Zhang,[1] Yao Zhang,[1] Yi Zhang,[9,j] Yu Zhang,[47] Z. H. Zhang,[6] Z. P. Zhang,[55] Z. Y. Zhang,[60] G. Zhao,[1] J. W. Zhao,[1,43] J. Y. Zhao,[1,47] J. Z. Zhao,[1,43] Lei Zhao,[55,43] Ling Zhao,[1] M. G. Zhao,[34] Q. Zhao,[1] S. J. Zhao,[63] T. C. Zhao,[1] Y. B. Zhao,[1,43] Z. G. Zhao,[55,43] A. Zhemchugov,[27,b] B. Zheng,[56] J. P. Zheng,[1,43] Y. Zheng,[35] Y. H. Zheng,[47] B. Zhong,[32] L. Zhou,[1,43] L. P. Zhou,[1,47] Q. Zhou,[1,47] X. Zhou,[60] X. K. Zhou,[47] X. R. Zhou,[55,43] Xiaoyu Zhou,[20] Xu Zhou,[20] A. N. Zhu,[1,47] J. Zhu,[34] J. Zhu,[44] K. Zhu,[1] K. J. Zhu,[1,43,47] S. H. Zhu,[54] W. J. Zhu,[34] X. L. Zhu,[45] Y. C. Zhu,[55,43] Y. S. Zhu,[1,47] Z. A. Zhu,[1,47] J. Zhuang,[1,43] B. S. Zou,[1] and J. H. Zou[1]

(BESIII Collaboration)

[1]*Institute of High Energy Physics, Beijing 100049, People's Republic of China*
[2]*Beihang University, Beijing 100191, People's Republic of China*
[3]*Beijing Institute of Petrochemical Technology, Beijing 102617, People's Republic of China*
[4]*Bochum Ruhr-University, D-44780 Bochum, Germany*
[5]*Carnegie Mellon University, Pittsburgh, Pennsylvania 15213, USA*
[6]*Central China Normal University, Wuhan 430079, People's Republic of China*
[7]*China Center of Advanced Science and Technology, Beijing 100190, People's Republic of China*
[8]*COMSATS University Islamabad, Lahore Campus,*
Defence Road, Off Raiwind Road, 54000 Lahore, Pakistan
[9]*Fudan University, Shanghai 200443, People's Republic of China*
[10]*G.I. Budker Institute of Nuclear Physics SB RAS (BINP), Novosibirsk 630090, Russia*
[11]*GSI Helmholtzcentre for Heavy Ion Research GmbH, D-64291 Darmstadt, Germany*
[12]*Guangxi Normal University, Guilin 541004, People's Republic of China*
[13]*Guangxi University, Nanning 530004, People's Republic of China*
[14]*Hangzhou Normal University, Hangzhou 310036, People's Republic of China*
[15]*Helmholtz Institute Mainz, Johann-Joachim-Becher-Weg 45, D-55099 Mainz, Germany*
[16]*Henan Normal University, Xinxiang 453007, People's Republic of China*
[17]*Henan University of Science and Technology, Luoyang 471003, People's Republic of China*
[18]*Huangshan College, Huangshan 245000, People's Republic of China*
[19]*Hunan Normal University, Changsha 410081, People's Republic of China*
[20]*Hunan University, Changsha 410082, People's Republic of China*
[21]*Indian Institute of Technology Madras, Chennai 600036, India*
[22]*Indiana University, Bloomington, Indiana 47405, USA*
[23a]*INFN Laboratori Nazionali di Frascati, I-00044, Frascati, Italy*
[23b]*INFN and University of Perugia, I-06100, Perugia, Italy*
[24a]*INFN Sezione di Ferrara, I-44122, Ferrara, Italy*
[24b]*University of Ferrara, I-44122, Ferrara, Italy*
[25]*Institute of Physics and Technology, Peace Ave. 54B, Ulaanbaatar 13330, Mongolia*
[26]*Johannes Gutenberg University of Mainz, Johann-Joachim-Becher-Weg 45, D-55099 Mainz, Germany*
[27]*Joint Institute for Nuclear Research, 141980 Dubna, Moscow region, Russia*
[28]*Justus-Liebig-Universitaet Giessen, II. Physikalisches Institut,*
Heinrich-Buff-Ring 16, D-35392 Giessen, Germany
[29]*KVI-CART, University of Groningen, NL-9747 AA Groningen, The Netherlands*
[30]*Lanzhou University, Lanzhou 730000, People's Republic of China*
[31]*Liaoning University, Shenyang 110036, People's Republic of China*
[32]*Nanjing Normal University, Nanjing 210023, People's Republic of China*
[33]*Nanjing University, Nanjing 210093, People's Republic of China*
[34]*Nankai University, Tianjin 300071, People's Republic of China*
[35]*Peking University, Beijing 100871, People's Republic of China*
[36]*Shandong Normal University, Jinan 250014, People's Republic of China*
[37]*Shandong University, Jinan 250100, People's Republic of China*
[38]*Shanghai Jiao Tong University, Shanghai 200240, People's Republic of China*
[39]*Shanxi University, Taiyuan 030006, People's Republic of China*
[40]*Sichuan University, Chengdu 610064, People's Republic of China*
[41]*Soochow University, Suzhou 215006, People's Republic of China*
[42]*Southeast University, Nanjing 211100, People's Republic of China*
[43]*State Key Laboratory of Particle Detection and Electronics,*
Beijing 100049, Hefei 230026, People's Republic of China
[44]*Sun Yat-Sen University, Guangzhou 510275, People's Republic of China*

[45]Tsinghua University, Beijing 100084, People's Republic of China
[46a]Ankara University, 06100 Tandogan, Ankara, Turkey
[46b]Istanbul Bilgi University, 34060 Eyup, Istanbul, Turkey
[46c]Uludag University, 16059 Bursa, Turkey
[46d]Near East University, Nicosia, North Cyprus, Mersin 10, Turkey
[47]University of Chinese Academy of Sciences, Beijing 100049, People's Republic of China
[48]University of Hawaii, Honolulu, Hawaii 96822, USA
[49]University of Jinan, Jinan 250022, People's Republic of China
[50]University of Manchester, Oxford Road, Manchester, M13 9PL, United Kingdom
[51]University of Minnesota, Minneapolis, Minnesota 55455, USA
[52]University of Muenster, Wilhelm-Klemm-Str. 9, 48149 Muenster, Germany
[53]University of Oxford, Keble Rd, Oxford, UK OX13RH
[54]University of Science and Technology Liaoning, Anshan 114051, People's Republic of China
[55]University of Science and Technology of China, Hefei 230026, People's Republic of China
[56]University of South China, Hengyang 421001, People's Republic of China
[57]University of the Punjab, Lahore-54590, Pakistan
[58a]University of Turin, I-10125, Turin, Italy
[58b]University of Eastern Piedmont, I-15121, Alessandria, Italy
[58c]INFN, I-10125, Turin, Italy
[59]Uppsala University, Box 516, SE-75120 Uppsala, Sweden
[60]Wuhan University, Wuhan 430072, People's Republic of China
[61]Xinyang Normal University, Xinyang 464000, People's Republic of China
[62]Zhejiang University, Hangzhou 310027, People's Republic of China
[63]Zhengzhou University, Zhengzhou 450001, People's Republic of China

Based on $(4.48 \pm 0.03) \times 10^8$ $\psi(3686)$ events, collected with the BESIII detector at the BEPCII storage ring, five h_c hadronic decays are searched for via the process $\psi(3686) \to \pi^0 h_c$. Three of them, $h_c \to p\bar{p}\pi^+\pi^-$, $\pi^+\pi^-\pi^0$, and $2(\pi^+\pi^-)\pi^0$, are observed for the first time with significances of 7.4σ, 4.6σ, and 9.1σ, and their branching fractions are determined to be $(2.89 \pm 0.32 \pm 0.55) \times 10^{-3}$, $(1.60 \pm 0.40 \pm 0.32) \times 10^{-3}$, and $(7.44 \pm 0.94 \pm 1.52) \times 10^{-3}$, respectively, where the first uncertainties are statistical and the second systematic. No significant signal is observed for the other two decay modes, and the corresponding upper limits of the branching fractions are determined to be $\mathcal{B}(h_c \to 3(\pi^+\pi^-)\pi^0) < 8.7 \times 10^{-3}$ and $\mathcal{B}(h_c \to K^+K^-\pi^+\pi^-) < 5.8 \times 10^{-4}$ at the 90% confidence level.

[a]Also at Bogazici University, 34342 Istanbul, Turkey
[b]Also at the Moscow Institute of Physics and Technology, Moscow 141700, Russia
[c]Also at the Functional Electronics Laboratory, Tomsk State University, Tomsk, 634050, Russia
[d]Also at the Novosibirsk State University, Novosibirsk, 630090, Russia
[e]Also at the NRC "Kurchatov Institute", PNPI, 188300, Gatchina, Russia
[f]Also at Istanbul Arel University, 34295 Istanbul, Turkey
[g]Also at Goethe University Frankfurt, 60323 Frankfurt am Main, Germany
[h]Also at Key Laboratory for Particle Physics, Astrophysics and Cosmology, Ministry of Education; Shanghai Key Laboratory for Particle Physics and Cosmology; Institute of Nuclear and Particle Physics, Shanghai 200240, People's Republic of China
[i]Also at Government College Women University, Sialkot—51310. Punjab, Pakistan.
[j]Also at Key Laboratory of Nuclear Physics and Ion-beam Application (MOE) and Institute of Modern Physics, Fudan University, Shanghai 200443, People's Republic of China
[k]Also at Harvard University, Department of Physics, Cambridge, MA, 02138, USA

The study of charmonium states is crucial for reaching a deeper understanding of the low-energy regime of quantum chromodynamics (QCD), a theory describing the strong interaction, which has been tested successfully at high energy. Since its discovery in 2005 [1,2], there have been few measurements of the decays of the spin-singlet charmonium state $h_c(^1P_1)$. Its best-measured decay is the radiative transition $h_c \to \gamma \eta_c$ [3–5], while the sum of the other known h_c decay branching fractions is less than 3% [6]. Among these measurements, there is only evidence for one h_c hadronic decay, $h_c \to 2(\pi^+\pi^-)\pi^0$, which was reported by CLEO-c with a statistical significance of 4.4σ [7].

Improved measurements and observation of new h_c hadronic-decay modes will shed light on the h_c decay mechanism, and be helpful for guiding the development of QCD based models. For example, perturbative QCD (pQCD) [8–10] and nonrelativistic QCD (NRQCD) [11–13] are two alternative models for describing features of low-energy QCD, and their predicted ratios of the hadronic width of the h_c to that of the η_c ($\Gamma_{h_c}^{\text{had}}/\Gamma_{\eta_c}^{\text{had}}$) are very different [14], as is the corresponding ratio involving decays of J/ψ mesons ($\Gamma_{h_c}^{\text{had}}/\Gamma_{J/\psi}^{\text{had}}$). New studies of h_c hadronic decays will enable these ratios to be measured, and comparisons to be made with the theoretical predictions.

The discovery of h_c hadronic decays provides new tag channels that can be used in XYZ (charmonium-like) studies with h_c as the intermediate state. This would provide a boost in signal yield comparable to that available from the tag channel $h_c \to \gamma \eta_c$, $\eta_c \to$ hadrons, which is the only mode applied at present.

Improved studies of h_c decays can be made with the large $\psi(3686)$ sample of 4.48×10^8 events [15], produced via e^+e^- collisions, which has been collected with the BESIII detector. In this paper, we report the first observations of decays $h_c \to p\bar{p}\pi^+\pi^-$, $\pi^+\pi^-\pi^0$, and $2(\pi^+\pi^-)\pi^0$, and upper limits of the branching ratios for the decays $h_c \to 3(\pi^+\pi^-)\pi^0$ and $K^+K^-\pi^+\pi^-$.

The BESIII detector [16] is a general purpose detector with a 93% solid angle coverage. A small-cell helium-based multilayer drift chamber (MDC) determines the momentum of charged particles in a 1 T magnetic field with a resolution of 0.5% at 1 GeV/c, and measures their ionization energy loss (dE/dx) with resolutions better than 6%. A CsI(T1) electromagnetic calorimeter (EMC) measures the photon energies with resolutions 2.5% (5.0%) in the barrel (end caps). A time-of-flight system (TOF), composed of plastic scintillators with resolution of 80 ps (110 ps) in the barrel (end caps), is used for particle identification (PID). A resistive plate chambers based muon counter with 2 cm position resolution is used for muon identification.

To obtain the detection efficiencies, signal Monte Carlo (MC) samples for the processes $\psi(3686) \to \pi^0 h_c$, and $h_c \to p\bar{p}\pi^+\pi^-$, $\pi^+\pi^-\pi^0$, $2(\pi^+\pi^-)\pi^0$, $3(\pi^+\pi^-)\pi^0$, or $K^+K^-\pi^+\pi^-$ are generated based on phase-space distributions. To investigate the background, an inclusive MC sample of 5.06×10^8 $\psi(3686)$ events is generated, in which the $\psi(3686)$ resonance is produced with KKMC [17,18]. Decays with known branching fractions obtained from the Particle Data Group (PDG) [6] are generated with EVTGEN [19], while the other decays are generated with LUNDCHARM [20]. In all the simulations, the GEANT4-based [21,22] package BOOST [23] is used to model the detector responses and to incorporate time-dependent beam backgrounds.

In the following, we denote decay modes $\psi(3686) \to \pi^0 h_c$ with $h_c \to p\bar{p}\pi^+\pi^-, \pi^+\pi^-\pi^0, 2(\pi^+\pi^-)\pi^0, 3(\pi^+\pi^-)\pi^0$, and $K^+K^-\pi^+\pi^-$ as modes I, II, III, IV, and V, respectively. Events are selected with the expected number of charged particle candidates, and at least two photon candidates for modes I and V, and four for modes II, III, and IV. Each charged track reconstructed in the MDC is required to be within 10 cm of the interaction point along the beam direction and 1 cm in the plane perpendicular to the beam. The polar angle θ of the tracks must be within the fiducial volume of the MDC ($|\cos\theta| < 0.93$). The TOF and dE/dx information of each charged track is used to calculate the corresponding probabilities of the hypotheses that a track is a pion, kaon or proton for particle identification. Electromagnetic showers are reconstructed by clustering energies deposited in the EMC, and in the nearby TOF counters. A photon candidate is such a shower with a deposited energy larger than 25 MeV in the barrel region ($|\cos\theta| < 0.8$) or 50 MeV in the end cap region ($0.86 < |\cos\theta| < 0.92$). The time t measured in the EMC with respect to the start of the event is required to be $0 < t < 700$ ns, to suppress electronic noise and beam-associated background. The angle between the photon and the extrapolated impact point in the EMC of the nearest charged track must be larger than $10°$ for charged pions and $20°$ for protons, respectively, to ensure that the cluster is not from that track.

Following the application of a vertex fit that constrains all the charged tracks to arise from a common interaction point, a kinematic fit is then performed to further improve resolution and suppress background. The kinematic fit applies constraints on the four-momentum conservation between initial and final states, and imposes the nominal π^0 mass [6] on $\gamma\gamma$ pairs within the interval $107 < M(\gamma\gamma) < 163$ MeV/c^2). If there is an excess of photon candidates in the event, then all combinations are considered and the one with the smallest χ^2 is kept. The χ^2 is required to be less than a specific value determined by maximizing $S/\sqrt{S+B}$, which is considered as a figure of merit (FOM). Here, S is the number of signal events from MC simulation normalized to the preliminary result measured with the unoptimized selection criteria and B is the number of background events extracted from the inclusive MC sample. The FOM is maximized in the h_c signal region

$|RM(\pi^0) - 3.525| < 8$ MeV/c^2, where $RM(\pi^0)$ is the recoiling mass of the π^0 meson, with the lower energy candidate chosen in the case of multiple π^0 s in the event.

To suppress contamination from decays with different numbers of photons to the signal modes, such as the dominant background decay $\psi(3686) \to \gamma\chi_{c2}$, where the χ_{c2} decays to the same final states as the h_c, $\chi^2_{4C.\,\mathrm{exp}} < \chi^2_{4C.\mathrm{unexp}}$ is required for each decay mode. Here $\chi^2_{4C.\,\mathrm{exp}}$ is obtained from the four-momentum kinematic fit that includes the expected number of photons in the signal candidate, i.e., two for modes I and V, and four for modes II, III, and IV, while $\chi^2_{4C.\mathrm{unexp}}$ is obtained from a fit including an unexpected number of photons, i.e., one for modes I and V, and three for modes II, III, and IV.

Mass windows, optimized simultaneously with the FOM, are applied to suppress the background contributions from $\psi(3686)$ decays to $\pi^0\omega$, $\pi^0\eta$, $\pi^0\pi^0 J/\psi$ and $\pi^+\pi^- J/\psi$, and are listed in Table I. The residual contamination is estimated with the inclusive MC sample.

Figure 1 shows the recoiling mass distribution of π^0_l, the lowest energy π^0 candidate, obtained by applying the above selection criteria. Clear h_c signals are observed in the modes $h_c \to p\bar{p}\pi^+\pi^-$, $\pi^+\pi^-\pi^0$, and $2(\pi^+\pi^-)\pi^0$, while no obvious signal is observed for $h_c \to 3(\pi^+\pi^-)\pi^0$ and $K^+K^-\pi^+\pi^-$. For the decay mode $h_c \to 2(\pi^+\pi^-)\pi^0$, there are $11.0 \pm 3.3 \pm 2.5$ peaking background events from $\psi(3686) \to \pi^0 h_c, h_c \to \gamma\eta_c$, where the first uncertainty is

TABLE I. Mass windows imposed in background rejection. M denotes the invariant mass $\sqrt{p^2}$, where p is the $\pi^+\pi^-\pi^0$ four momentum. RM denotes the recoiling mass $\sqrt{(p_{\psi(3686)} - p)^2}$, where $p_{\psi(3686)}$ is the $\psi(3686)$ four momentum, and p is the $\pi^+\pi^-$, $\pi^0\pi^0$, or π^0 four momentum. m denotes the nominal mass [6] of the indicated particle. π^0_l (π^0_h) denotes the π^0 candidate with lower (higher) energy.

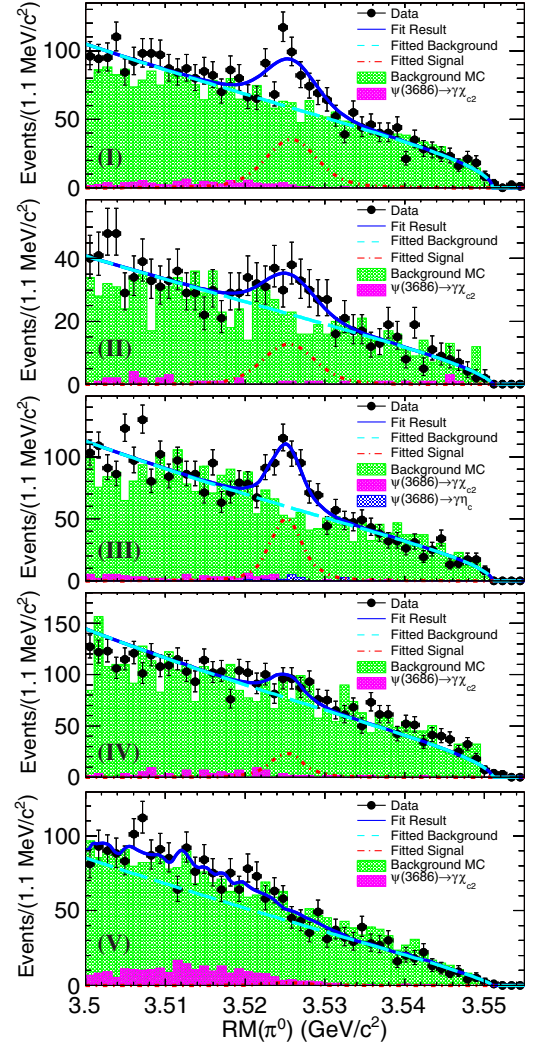| Mode	Mass windows (MeV/c^2)
I	$\|RM(\pi^+\pi^-) - m(J/\psi)\| > 18$
	$\|M(\pi^+\pi^-\pi^0) - m(\eta)\| > 14$
	$\|M(\pi^+\pi^-\pi^0) - m(\omega)\| > 6$
II	$\|RM(\pi^0_l\pi^0_h) - m(J/\psi)\| > 74$
	$\|RM(\pi^0_h) - m(\omega)\| > 32$
III	$\|RM(\pi^0_l\pi^0_h) - m(J/\psi)\| > 20$
	$\|RM(\pi^+\pi^-) - m(J/\psi)\| > 22$
	$\|M(\pi^+\pi^-\pi^0_l) - m(\eta)\| > 16$
	$\|M(\pi^+\pi^-\pi^0_l) - m(\omega)\| > 20$
IV	$\|RM(\pi^0_l\pi^0_h) - m(J/\psi)\| > 18$
	$\|RM(\pi^+\pi^-) - m(J/\psi)\| > 20$
	$\|M(\pi^+\pi^-\pi^0_l) - m(\eta)\| > 16$
V	$\|RM(\pi^+\pi^-) - m(J/\psi)\| > 22$
	$\|M(\pi^+\pi^-\pi^0) - m(\eta)\| > 16$
	$\|M(\pi^+\pi^-\pi^0) - m(\omega)\| > 20$

FIG. 1. Recoiling mass spectra of the lowest energy π^0, in the decay chains $\psi(3686) \to \pi^0 h_c$ with $h_c \to p\bar{p}\pi^+\pi^-$ (I), $\pi^+\pi^-\pi^0$ (II), $2(\pi^+\pi^-)\pi^0$ (III), $3(\pi^+\pi^-)\pi^0$ (IV), and $K^+K^-\pi^+\pi^-$ (V). In each spectrum, the dots with error bars represent data, the pink shaded histogram is the background process $\psi(3686) \to \gamma\chi_{c2}$, the blue filled histogram is the background process $\psi(3686) \to \pi^0 h_c, h_c \to \gamma\eta_c$, the green filled histogram is the background from inclusive MC, the cyan dashed curve is the fitted background, the red dash-dotted curve is the fitted signal, and the blue curve is the fitted result.

statistical and the second systematic, while no peaking background is found for the other decay modes, based on inclusive MC. The remaining background from $\psi(3686) \to \gamma\chi_{c2}$ is negligible for all the decay modes except $h_c \to K^+K^-\pi^+\pi^-$, which will therefore be considered separately in the fit below. The background contributions from the continuum processes are studied with a 44 pb^{-1} data set taken at $\sqrt{s} = 3650$ MeV, which yields no h_c candidates in any of the final states analyzed.

To obtain the number of signal events, an unbinned maximum likelihood fit is performed to the corresponding mass spectrum, as shown in Fig. 1. In each fit, the signal is

TABLE II.   Results of the analysis. Here ϵ denotes the selection efficiency, N_{h_c} denotes the h_c signal yield, $\mathcal{B}_{\psi(3686)}$ and $\mathcal{B}_{h_c}$ denote the branching fraction $\mathcal{B}(\psi(3686) \to \pi^0 h_c)$ and $\mathcal{B}(h_c \to \text{hadrons})$, respectively, S.S. is the significance of the signal peak, including systematic uncertainties, and $\mathcal{B}_{h_c}^{\text{PDG}}$ denotes the branching fraction of $h_c \to$ hadrons from the PDG [6]. Only statistical uncertainties are presented for signal yields, while for the (product) branching fractions, the first uncertainty is statistical and the second systematic. For the decay mode $h_c \to 3(\pi^+\pi^-)\pi^0$ both the branching fraction and upper limit are listed.

Mode		$\epsilon(\%)$	N_{hc}	$\mathcal{B}_{\psi(3686)} \times \mathcal{B}_{h_c}(10^{-6})$	$\mathcal{B}_{h_c}(10^{-3})$	S.S.	$\mathcal{B}_{h_c}^{\text{PDG}}(10^{-3})$
I	$h_c \to p\bar{p}\pi^+\pi^-$	20.9	230 ± 25	$2.49 \pm 0.27 \pm 0.28$	$2.89 \pm 0.32 \pm 0.55$	7.4σ	$\cdots$
II	$h_c \to \pi^+\pi^-\pi^0$	16.8	101 ± 25	$1.38 \pm 0.35 \pm 0.17$	$1.60 \pm 0.40 \pm 0.32$	4.6σ	<2.2
III	$h_c \to 2(\pi^+\pi^-)\pi^0$	9.1	254 ± 32	$6.40 \pm 0.81 \pm 0.87$	$7.44 \pm 0.94 \pm 1.52$	9.1σ	22^{+8}_{-7}
IV	$h_c \to 3(\pi^+\pi^-)\pi^0$	4.2	73 ± 34	$4.00 \pm 1.87 \pm 0.70$	$4.65 \pm 2.17 \pm 1.08$	2.1σ	<29
			<136	<7.5	<8.7	$\cdots$	
V	$h_c \to K^+K^-\pi^+\pi^-$	18.1	<40	<0.5	<0.6	$\cdots$	$\cdots$

described with the MC simulated shape convoluted with a Gaussian function, and the background is described with an ARGUS function [24], except for the mode $h_c \to K^+K^-\pi^+\pi^-$, where an additional background component from $\psi(3686) \to \gamma\chi_{c2}, \chi_{c2} \to K^+K^-\pi^+\pi^-$ is included. Here, the MC shape includes the intrinsic h_c line shape and detection resolution, while the Gaussian function accounts for the discrepancy between data and MC simulation in the mass resolution. All the parameters of the Gaussian and ARGUS functions, except the threshold value of 3551 MeV/c^2, are floated in the fit.

Branching fractions are calculated based on the formula,

$$\mathcal{B}_{h_c} = \frac{N_{h_c}}{\mathcal{B}(\psi(3686) \to \pi^0 h_c) \cdot \mathcal{B}(\pi^0 \to \gamma\gamma) \cdot N_{\psi(3686)} \cdot \epsilon},$$

(1)

where $\mathcal{B}_{h_c}$ represents the branching fraction of the given signal mode, while $\mathcal{B}(\psi(3686) \to \pi^0 h_c)$ and $\mathcal{B}(\pi^0 \to \gamma\gamma)$ are the branching fractions of $\psi(3686) \to \pi^0 h_c$ and $\pi^0 \to \gamma\gamma$, respectively, N_{h_c} and $N_{\psi(3686)}$ are the numbers of h_c signal and $\psi(3686)$ events, respectively, and ϵ is the selection efficiency obtained from signal MC simulation. Since no significant signal is observed in the decays $h_c \to K^+K^-\pi^+\pi^-$ and $3(\pi^+\pi^-)\pi^0$, their upper limits are determined with a Bayesian method [25]. With the fit function described before, we scan the number of signal yield to obtain the likelihood distribution, and smear it with the systematic uncertainties. The upper limits of the number of signal yield $N_{h_c}^{up}$ at the 90% confidence level are obtained via $\int_0^{N_{h_c}^{up}} F(x)dx / \int_0^\infty F(x)dx = 0.90$, where $F(x)$ is the probability density function of the likelihood distribution. All the numerical results, including selection efficiencies, signal yields, branching fractions or upper limits and significances, are listed in Table II.

The sources of systematic uncertainties for the product branching fractions include tracking, photon and π^0 reconstruction, PID, the kinematic fit, the number of $\psi(3686)$ events, fitting procedure, η_c peaking background, mass windows and the physics model describing the h_c production and decay dynamics. All the systematic uncertainties are summarized in Table III, and the overall systematic uncertainties are obtained by summing all individual components in quadrature. In addition, we add a relative systematic uncertainty of 15.2% associated with the branching fraction of $\psi(3686) \to \pi^0 h_c$ in calculating the branching fraction of the h_c hadronic decays.

The uncertainties on the tracking efficiency are estimated with the control samples $\psi(3686) \to \pi^+\pi^- J/\psi$, $J/\psi \to K_S^0 K^\pm \pi^\mp$ and $\psi(3686) \to p\bar{p}\pi^+\pi^-$, and are determined to be 1.0% [26], 1.0% [27], 1.3%, and 1.7% for each charged pion, kaon, proton, and antiproton, respectively. The uncertainties on the photon and π^0 reconstruction efficiency are studied using the control sample $J/\psi \to \pi^+\pi^-\pi^0$, and are determined to be 1.0% per photon [28] and 1% per π^0 [28]. The PID uncertainties are determined to be 1.0% per pion [29], 1.0% per kaon [27], 1.3% per proton and 1.6% per antiproton, based on the same samples used to estimate tracking uncertainties. The uncertainty associated with the kinematic fit is estimated by comparing the efficiencies with and without the helix parameter correction [30].

TABLE III.   Relative uncertainties (in %) on the branching fractions.

Source	I	II	III	IV	V
Tracking	5.0	2.0	4.0	6.0	4.0
Photon	2.0	4.0	4.0	4.0	2.0
π^0 reconstruction	1.0	2.0	2.0	2.0	1.0
PID	4.9	2.0	4.0	6.0	4.0
Kinematic fit	1.8	2.2	3.7	4.2	1.5
Number of $\psi(3686)$	0.7	0.7	0.7	0.7	0.7
Fitting range	2.6	3.5	4.9	$\cdots$	$\cdots$
Signal shape	1.3	8.1	2.5	$\cdots$	$\cdots$
Background shape	2.1	3.5	2.9	$\cdots$	$\cdots$
Resolution	4.2	5.1	3.3	$\cdots$	$\cdots$
η_c	$\cdots$	$\cdots$	1.5	$\cdots$	$\cdots$
Physics model	6.3	2.6	8.2	14.1	7.3
Sum	11.3	12.5	13.6	17.6	9.6

TABLE IV. The ratios of the hadronic decay widths of h_c to η_c ($\Gamma_{h_c}^{\text{had}}/\Gamma_{\eta_c}^{\text{had}}$) and h_c to J/ψ ($\Gamma_{h_c}^{\text{had}}/\Gamma_{J/\psi}^{\text{had}}$). The theoretical predictions of the total hadronic decay ratios are based on pQCD and NRQCD [14], which are expected to be correct also for exclusive decay modes. The experimental measurements of the ratios of the partial decay widths for $p\bar{p}\pi^+\pi^-$, $K^+K^-\pi^+\pi^-$, and $n(\pi^+\pi^-)\pi^0(n=0,1,2)$ modes are calculated based on the measured branching fractions in this analysis and the PDG [6].

	Model/mode	Ratio
$\Gamma_{h_c}^{\text{had}}/\Gamma_{\eta_c}^{\text{had}}$	pQCD	0.010 ± 0.001
	NRQCD	0.083 ± 0.018
	$p\bar{p}\pi^+\pi^-$	0.012 ± 0.008
	$K^+K^-\pi^+\pi^-$	<0.083
$\Gamma_{h_c}^{\text{had}}/\Gamma_{J/\psi}^{\text{had}}$	pQCD	0.68 ± 0.07
	NRQCD	8.03 ± 1.31
	$p\bar{p}\pi^+\pi^-$	3.63 ± 2.25
	$\pi^+\pi^-\pi^0$	0.57 ± 0.38
	$2(\pi^+\pi^-)\pi^0$	1.43 ± 0.90
	$3(\pi^+\pi^-)\pi^0$	<2.26
	$K^+K^-\pi^+\pi^-$	<0.68

The uncertainty on the number of $\psi(3686)$ events is 0.7%, according to the study in Ref. [15].

The fitting range, signal and background descriptions, and the difference in resolution between data and simulation are considered as sources of systematic uncertainty related to the fitting procedure. These uncertainties are assigned by varying the boundaries of the fitting ranges by ± 10 MeV/c^2, changing the signal description from the shape determined from the simulation to a Breit-Wigner function, and replacing the ARGUS function describing the background with a second-order Chebychev polynomial. The difference between the results obtained by fixing and releasing the resolution in the fit is taken as the uncertainty on the knowledge of this quantity, where in the former case a correction of 1 MeV/c^2 is first applied to the value from the simulation, as determined from a control sample $\psi(3686) \to \gamma\chi_{c1} \to \gamma p\bar{p}\pi^+\pi^-$. For $h_c \to 3(\pi^+\pi^-)\pi^0$ and $K^+K^-\pi^+\pi^-$, the largest upper limits are taken with different combinations of fitting models and ranges. The uncertainty due to η_c peaking background is assigned from the statistical uncertainty on the fit result for this component, and the corresponding uncertainty on the branching fractions.

A systematic uncertainty due to the physics model arises from the limited knowledge of the intermediate states in h_c decays. Searches have been performed for intermediate states contributing to modes I to III, which are detailed in the Supplemental Material [31]. Possible contributions are found for several such states, which include a ρ^0 peak in each projection of the $\pi^+\pi^-$ invariant mass. The effect of these states on the selection efficiency is evaluated by generating alternative simulation samples with different properties and comparing with the default production.

In summary, three h_c hadronic decays, $h_c \to p\bar{p}\pi^+\pi^-$, $h_c \to \pi^+\pi^-\pi^0$, and $h_c \to 2(\pi^+\pi^-)\pi^0$, are observed for the first time, and two channels, $h_c \to K^+K^-\pi^+\pi^-$ and $h_c \to 3(\pi^+\pi^-)\pi^0$, are searched for. The measured branching fractions or upper limits, as well as the significance of the signal peaks, are listed in Table II. The measured branching fraction of $h_c \to 2(\pi^+\pi^-)\pi^0$ is more precise than the CLEO-c result [7] and lower in value, although consistent within uncertainties. The sum of the branching fractions of the three observed channels is approximately 1.2%, which is still smaller than the h_c radiative transition to the η_c, and does not yet allow a conclusion on whether the total hadronic decay width of the h_c is of the same order as its radiative transition. Table IV shows the comparisons of the measured ratios of the hadronic decay widths $\Gamma_{h_c}^{\text{had}}/\Gamma_{\eta_c}^{\text{had}}$ and $\Gamma_{h_c}^{\text{had}}/\Gamma_{J/\psi}^{\text{had}}$ and the theoretical predictions. The experimental results tend to favor the lower predictions, which come from pQCD. However, in Ref. [14], the theoretical prediction of $\mathcal{B}(h_c \to \gamma\eta_c) = (41 \pm 3)\%$ based on NRQCD is favored by the experimental measurement $(51 \pm 6)\%$ [6], compared with the prediction of $(88 \pm 2)\%$ from pQCD. We note that the experimental measurements are still limited by low statistics and the predictions of the theoretical models can be modified through considerations such as normalization scale or relativistic corrections [32,33]. Future experimental measurements of higher precision, and improved theoretical calculations will help to resolve this inconsistency.

ACKNOWLEDGMENTS

[1] P. Rubin *et al.* (CLEO Collaboration), Phys. Rev. D **72**, 092004 (2005).

[2] J. L. Rosner *et al.* (CLEO Collaboration), Phys. Rev. Lett. **95**, 102003 (2005).

[3] M. Andreotti *et al.* (Fermilab E835 Collaboration), Phys. Rev. D **72**, 032001 (2005).

[4] S. Dobbs *et al.* (CLEO Collaboration), Phys. Rev. Lett. **101**, 182003 (2008).

[5] M. Ablikim *et al.* (BESIII Collaboration), Phys. Rev. Lett. **104**, 132002 (2010).

[6] M. Tanabashi *et al.* (Particle Data Group), Phys. Rev. D **98**, 030001 (2018).

[7] G. S. Adams *et al.* (CLEO Collaboration), Phys. Rev. D **80**, 051106 (2009).

[8] A. Duncan and A. H. Mueller, Phys. Lett. **93B**, 119 (1980).

[9] S. J. Brodsky and G. P. Lepage, Phys. Rev. D **24**, 2848 (1981).

[10] V. N. Baier and A. G. Grozin, Z. Phys. C **29**, 161 (1985).

[11] W. E. Caswell and G. P. Lepage, Phys. Lett. **167B**, 437 (1986).

[12] G. P. Lepage, L. Magnea, C. Nakhleh, U. Magnea, and K. Hornbostel, Phys. Rev. D **46**, 4052 (1992).

[13] G. T. Bodwin, E. Braaten, and G. P. Lepage, Phys. Rev. D **51**, 1125 (1995).

[14] Y. P. Kuang, Phys. Rev. D **65**, 094024 (2002).

[15] M. Ablikim *et al.* (BESIII Collaboration), Chin. Phys. C **42**, 023001 (2018).

[16] M. Ablikim *et al.* (BESIII Collaboration), Nucl. Instrum. Methods Phys. Res., Sect. A **614**, 345 (2010).

[17] S. Jadach, B. F. L. Ward, and Z. Was, Comput. Phys. Commun. **130**, 260 (2000).

[18] S. Jadach, B. F. L. Ward, and Z. Was, Phys. Rev. D **63**, 113009 (2001).

[19] R. G. Ping, Chin. Phys. C **32**, 243 (2008).

[20] J. C. Chen, G. S. Huang, X. R. Qi, D. H. Zhang, and Y. S. Zhu, Phys. Rev. D **62**, 034003 (2000).

[21] S. Agostinelli *et al.* (GEANT4 Collaboration), Nucl. Instrum. Methods Phys. Res., Sect. A **506**, 250 (2003).

[22] J. Allison *et al.*, IEEE Trans. Nucl. Sci. **53**, 270 (2006).

[23] Z. Y. Deng *et al.*, HEP & NP **30**, 371 (2006).

[24] H. Albrecht *et al.* (ARGUS Collaboration), Phys. Lett. B **340**, 217 (1994).

[25] G. J. Feldman and R. D. Cousins, Phys. Rev. D **57**, 3873 (1998).

[26] M. Ablikim *et al.* (BESIII Collaboration), Phys. Rev. Lett. **105**, 261801 (2010).

[27] M. Ablikim *et al.* (BESIII Collaboration), Phys. Rev. D **83**, 112005 (2011).

[28] M. Ablikim *et al.* (BESIII Collaboration), Phys. Rev. D **81**, 052005 (2010).

[29] M. Ablikim *et al.* (BESIII Collaboration), Phys. Rev. D **86**, 092009 (2012).

[30] M. Ablikim *et al.* (BESIII Collaboration), Phys. Rev. D **87**, 012002 (2013).

[31] See Supplemental Material at http://link.aps.org/supplemental/10.1103/PhysRevD.99.072008 for searches of the intermediate states in $h_c \to p\bar{p}\pi^+\pi^-$, $\pi^+\pi^-\pi^0$, and $2(\pi^+\pi^-)\pi^0$.

[32] Q. L. Zhang, X. G. Wu, X. C. Zheng, S. Q. Wang, H. B. Fu, and Z. Y. Fang, Chin. Phys. Lett. **31**, 051202 (2014).

[33] J. Z. Li, Y. Q. Ma, and K. T. Chao, Phys. Rev. D **88**, 034002 (2013).